13th ewtec 2019 Proceedings of the 13th European Wave and Tidal Energy Conference 1-6 Sept 2019, Naples, Italy

Turbulent flow mapping around a floating in-stream tidal energy platform

Maricarmen Guerra, Alex E. Hay, Richard A. Cheel, Greg Trowse, and Richard Karsten

***Abstract*—In this investigation instrumented mobile platforms are used to spatially map turbulent flows in Grand Passage, a tidal channel in Nova Scotia, Canada. Specifically, the measurements aim to characterize the flow around the PLAT-I floating tidal energy platform developed by Sustainable Marine Energy (SME). GPS-tracked surface drifters equipped with fast-sampling Acoustic Doppler current profilers (ADCPs) provide turbulence-resolving vertical profiles of velocity along the drifter trajectory. Controlled transect measurements using vessel-mounted ADCPs capture inflow conditions and across-platform's wake data. These data are used to obtain estimates of the mean flow and turbulence parameters as a function of position both within and outside the platform's wake.**

***Index Terms*—tidal energy, turbulence, turbine wake, acoustic Doppler profiler, drifting buoy**

I. Introduction

FULL-SCALE hydrokinetic turbines are being deployed at different sites around the world. Mean-flow conditions are typically used for resource characterization, while ambient turbulence is used in hydrokinetic turbine design as it impacts their performance and durability. Once turbines are deployed and extracting energy, wake-induced turbulence impacts the flow around the turbines and becomes critical for the design of turbine arrays [1]–[4]. As such, the success of these full-scale turbine deployments requires accurate mapping in the field of the turbulent inflow conditions and of the real impacts of energy extraction causes on the natural environment [5]–[8]. However, turbines are typically installed in sites with strong currents, where field measurements are challenging and expensive, and the use of multiple moored instruments does not provide enough spatial resolution. Hence, efficient field methods that can accurately map both the spatial and temporal structure of these turbulent flows are needed.

Acoustic Doppler current profilers (ADCPs) are the instrument of choice for measuring ocean currents. Vessel-mounted ADCPs are typically used for spatial mapping of mean flow velocities. Turbulence parameters such as turbulent kinetic energy dissipation rates and Reynolds stresses can be estimated if the single-ping along-beam velocities are retained and Doppler noise variance is removed from the measurements [9]–[11].

New fast-sampling profilers (up to 16 Hz) allow for accurate (low-noise) turbulence measurements through the water column [12], [13]. This capability also expands their use for spatial mapping of turbulence in fast flows. For example, an ADCP drifting freely in a 3 m s^{-1} current, can capture a velocity profile every 0.75 m (horizontally) when sampling at 4Hz. Drifting buoys equipped with ADCPs have been successfully used to measure upper-ocean turbulence in [14], [15]. A drifting Nortek Signature1000 ADCP (sampling at 8 Hz in a 2.5 m s^{-1} current) was successfully used to map mean-flow and turbulences parameters both within and outside of the wake of an hydrokinetic turbine on steady flow in [16].

Turbine wakes are typically characterized by slower velocities (because momentum has been extracted from the flow), and increased turbulence (due to blockage and eddy shedding from the rotating blades and turbine support structure [17]). Wake extent, evolution, and possible recovery, depend on the turbine design, blockage ratio, and ambient flow conditions, such as shear, turbulence, and proximity to the boundaries. Most hydrokinetic turbine wake studies have been conducted at the numerical and laboratory scale [18]–[20], mainly differing on the detailed representation of the turbines and ambient flows. Only a few wake studies are available at the field scale [16], [21].

In this investigation ADCPs mounted on both propelled and freely-drifting mobile surface platforms are used to spatially map unsteady turbulent flows in Grand Passage, Nova Scotia, Canada, expanding the method used in [16] for steady flows. Measurements are conducted around the PLAT-I floating tidal energy platform developed by Sustainable Marine Energy (SME) [22]. The end goal of the project is to characterize the combined wake of four turbines to be installed on-board PLAT-I. This paper presents measurements around the platform collected prior to turbine blades installation. Section II describes the study site and data collection methods. Section III presents a summary of the data collected up to date, and estimated mean-flow and turbulence parameters. Finally, conclusion and future work are presented in Section IV.

II. Methods

A. Study Site

Grand Passage is a tidal channel located in the south-east of Bay of Fundy, Nova Scotia, Canada (N 44.27°;

Paper ID 1482, Tidal resource characterization track, 13th European Wave and Tidal Energy Conference, Napoli, Italy, 2019. This research is supported by the Offshore Energy Research Association of Canada and the Canada Foundation for Innovation.

M. Guerra, A. E. Hay, and R. A. Cheel are with Dalhousie University, Department of Oceanography, 1355 Oxford Street, Halifax, NS, B3H 4R2, Canada (e-mail: mguerra@dal.ca, alex.hay@dal.ca, and richard.cheel@dal.ca).

G. Trowse is with Luna Ocean Consulting Ltd., Halifax, NS, Canada (e-mail: greg.trowse@lunaocean.ca).

R. Karsten is with Acadia University, Department of Mathematics and Statistics, 2 University Ave., Wolfville, NS, B4P 2R6, Canada (e-mail: richard.karsten@acadiau.ca)

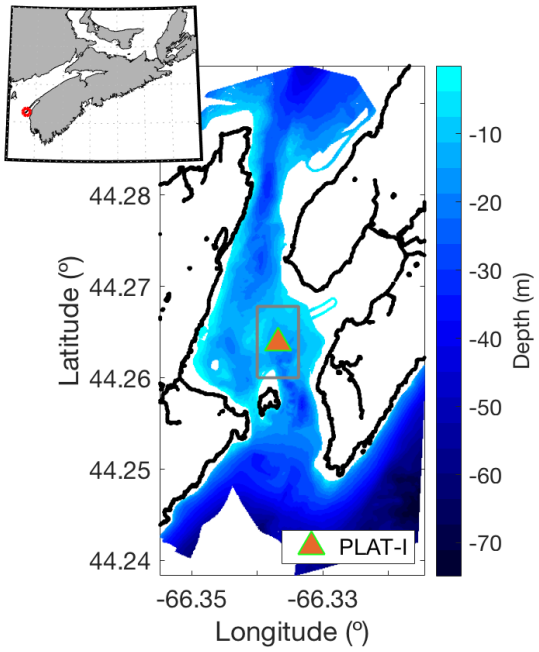

Fig. 1. Grand Passage map colored by bathymetry. The triangle corresponds to PLAT-I location in Grand Passage. The grey rectangle shows the measurements area. The black line corresponds to the coastline. The inset plot shows the province of Nova Scotia, Canada, and the red dot shows Grand Passage location in the south of Bay Fundy.

W 66.34°). The channel axis runs approximately to the north-south, separating Long Island (to the east) and Brier Island (to the west). Grand Passage is about 4 km long and 1.5 km wide at the measurement location. Grand Passage has been previously selected for tidal energy extraction due to its strong tidal currents (∼3 m s^{-1}) [23]. Fig. 1 shows a map of Grand Passage colored by bathymetry and the location of the channel with respect to Bay of Fundy and Nova Scotia. Flood tidal currents are northward.

Numerical predictions of velocity from an FVCOM model of model of Digby Neck area developed by Acadia University [23], [24] are shown in Fig. 2 for the area surrounding PLAT-I (grey box in Fig. 1). These plots correspond to peak flood and peak ebb on November 19th and 20th 2018, and illustrate how velocities vary spatially at this location. Slower velocities observed in the southwest corner during flood (Fig. 2a) correspond to the wake of Peter's Island. At the study site, velocity principal direction is about 18.8° CCW from north (obtained from model predictions).

B. Turbine platform: PLAT-I

Sustainable Marine Energy (SME) PLAT-I (Fig. 3) is a three-hulled floating platform designed to support four horizontal-axis hydrokinetic turbines along its cross-deck. The platform is about 30 m long (center hull) and 30 m wide (cross-deck). The platform is 2-point moored, and it self-aligns with the incoming flow, thus the turbines face the tidal currents at all times [22]. The platform, with four 4 m diameter Schottel Hydro turbines, was previously deployed and tested in Connell, Scotland [22], [25]. PLAT-I was deployed in Grand Passage, Nova Scotia in September 2018 to

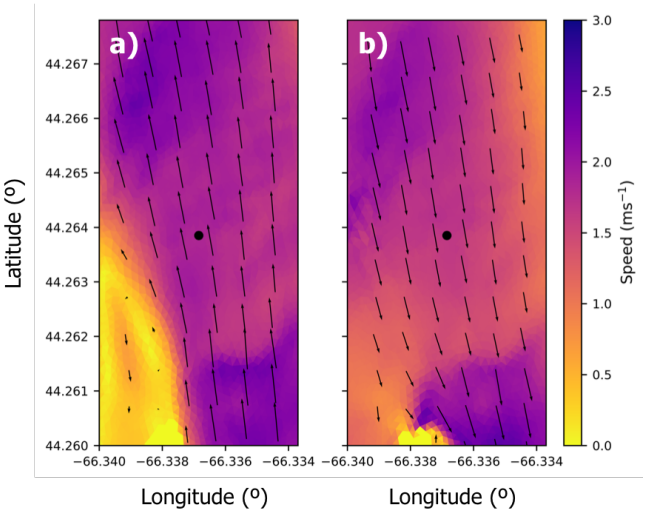

Fig. 2. Model-predicted speed and velocity direction in the area surrounding PLAT-I (grey box on Fig. 1): a) Peak flood on November 19th and b) peak ebb on November 20th 2018. Arrows are plotted every 75 m. Note model resolution is ∼20 m. Black dot shows PLAT-I location.

Fig. 3. PLAT-I deployed in Grand Passage, Nova Scotia. The four turbines' support structures are visible along the platform cross-deck. In this picture, turbine blades are not installed. Visible in this picture is the surface expression of the platform wake. Photo by Greg Trowse.

the north of Peter's Island (N 44.2639°; W 66.3369°). The Nova Scotia version of PLAT-I will support four 6.3 m diameter Schottel Hydro turbines, each rated at 280 kW and designed for a maximum flow speed of 4 m s^{-1}.

C. Data Collection

Flow velocity data were collected upstream and downstream PLAT-I prior to the installation of turbine blades on November 19th and 20th 2018 (three days after neap tides). During these days, wind speeds were below 4 knots, and there were no significant surface-gravity waves. There were two sets of measurements: streamline following drifts and underway vessel transects. Table I summarizes the instrument settings.

A surface drifter was used to measure turbulence-resolving velocity profiles through the water column along the drifter trajectory. A Nortek Signature 500

TABLE I
SUMMARY OF DEPLOYMENTS AND SAMPLING PARAMETERS AT GRAND PASSAGE

Instrument	Nortek Signature 500 kHz	RDI Workhorse 300 kHz
Platform	Drifter	Puffin
Sampling Frequency (Hz)	4	1
Δz (m)	0.6	0.5
Distance to first bin (m)	1.1	1.6
Range (m)	40.1	46.6

Fig. 4. Drifter buoy with GPS case and down-looking Nortek Signature 500 deployed in Grand Passage.

kHz five-beam acoustic Doppler current profiler was installed down-looking on a HDPE structure and mounted on a disk buoy for additional buoyancy (See Fig. 4). The Signature was set to record single-ping along-beam velocities every 0.6 m using its five beams at 4 Hz (the maximum possible for continuous sampling using all beams). Single-ping error for the along-beam velocities reported by the instrument manufacturer for these settings is 0.08 m s^{-1}. The drifter buoy was equipped with one Garmin 78s GPS receiver, which recorded drifter position at 1 Hz.

Drifts began just downstream the platform location (almost next to the hulls) by releasing the drifter from a small vessel, the Puffin. The drifter was released at different positions across the PLAT-I width for both ebb and flood tides. Each drift lasted at least 90 s (the distance varied depending on tidal stage). There were 29 ebb tide drifts and 6 flood tide drifts.

Data were quality controlled to remove low correlation (below 50) and low amplitude (below 50 dB) data. At the beginning of each drift, mooring chain reflection contaminated the Signature velocity measurements, thus the first 10 seconds of drifting data were removed from the drift tracks.

Fig. 5 shows pitch and roll spectra recorded by the attitude and heading reference system (AHRS) onboard the Signature along each drift track. The accelerometer spectra (not shown) exhibit similar structure. The peak at 1 s is likely associated with the drifter response to the variable sea surface roughness (associated with large-scale turbulent eddies), rather than with wind-generated surface gravity waves. For the analysis presented here, the effect of these motions on the vertical

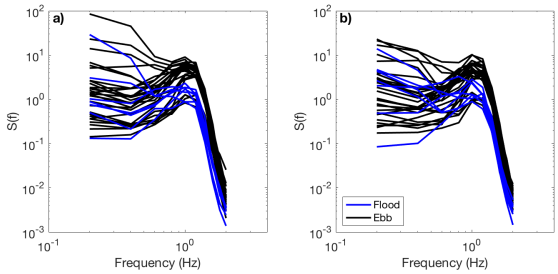

Fig. 5. a) Pitch and b) roll spectra estimated from attitude parameters recorded by the Signature AHRS along drift tracks. Note peak at 1 Hz.

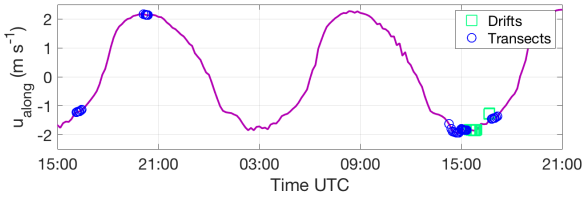

Fig. 6. Surface along-channel velocity at PLAT-I location (prediction) for November 19 and 20 2018. Blue circles and green squares represent drift and transect begin times respectively.

velocities recorded along the Signature's vertical beam was corrected to first order by subtracting the vertical mean. This correction was effective in removing vertical "banding" in the raw vertical velocity data. Banding which was more pronounced on ebb than flood, and was clearly an artifact associated with the bobbing motion of the buoy.

Controlled transects were conducted on ebb tide on November 20th 2018. An RDI Workhorse 600 kHz ADCP was mounted down-looking on board the Puffin. A Garmin 78s GPS receiver recorded vessel position at 1 Hz (synchronized with the ADCP). The Workhorse was set to measure along-beam velocities sampling at 1 Hz every 0.5 m; the first bin was at 1.6 m below the free-surface. Bottom-track velocities were measured to estimate true water velocities.

Fig. 6 shows the predicted of along-channel surface velocity at the platform location during this field campaign together with drifts and transects start times. Currents were about 2 m s^{-1} during the measurements, and most drifts and transects occurred during peak tidal flow for those days.

A local coordinate system is defined for data organization purposes. The origin is defined at the PLAT-I center location (the platform moves along an ellipse as the tidal currents change in magnitude and direction [22]). The y-axis corresponds to the along-channel principal direction of the currents at this site (18.8° CCW from north, positive northward), while the x-axis corresponds to the cross-channel principal direction of the flow (positive eastward). Fig. 7 shows drift trajectories and transects in this local coordinate system. All drifts occurred downstream of PLAT-I, thus all flood drifts flow on a positive y direction, while all ebb drifts flow in the negative y direction. Drift trajectories are colored by average drifting velocity (obtained from the GPS measurements). Averaged drifting velocity ranged

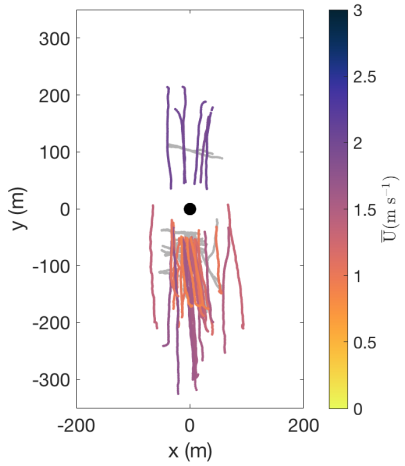

Fig. 7. All drift tracks colored by average drifting velocity $\overline{U}$, and selected transects in grey. Black dot represents center Plat-I location.

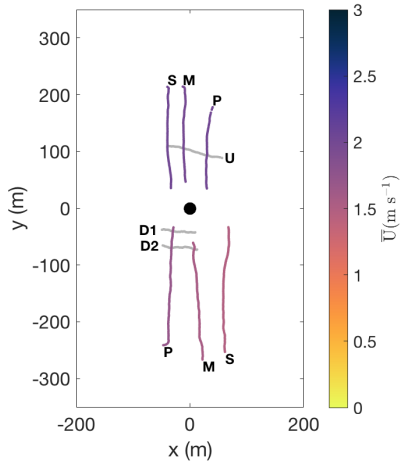

Fig. 8. Selected ebb and flood drift tracks colored by average drifting velocity, and selected transects in grey. Black dot represents center Plat-I location.

from 1 to 1.8 m s^{-1}.

III. Flow Measurements

Flow velocities are presented for the selected drifts and transects shown in Fig. 8. Selected drifts were collected at the starboard (S), middle (M), and port (P) side of PLAT-I, while selected transects were collected upstream (U) and downstream (D1, D2) of PLAT-I during ebb tide.

D. Drifts

As the drifter is transported by the flow at the surface, the Signature captures horizontal velocity fluctuations with respect to the surface drifting velocity. Vertical profiles of eulerian horizontal velocities are constructed by combining both measurements, such that:

$$u(x,y,z,t) = u_{\text{GPS}}(x,y,t) + u_{\text{Sig}}(x,y,z,t), \quad (1)$$

$$v(x,y,z,t) = v_{\text{GPS}}(x,y,t) + v_{\text{Sig}}(x,y,z,t), \quad (2)$$

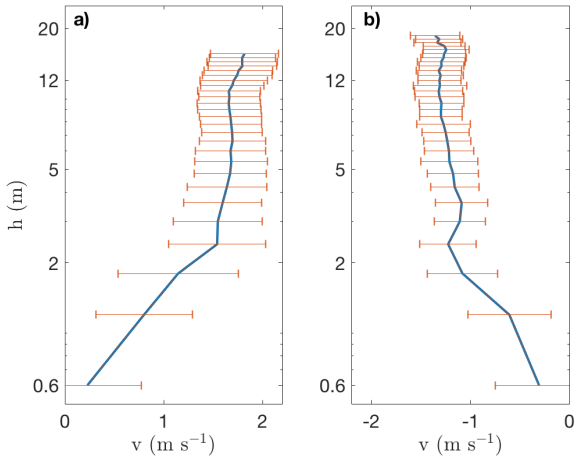

Fig. 9. Averaged vertical profiles of along-channel velocity and standard deviation for middle drifts at a) flood tide, and b) ebb tide. Note that on these plots the vertical axis corresponds to distance from the bottom.

where u and v correspond to the horizontal components of velocity in the local coordinate system (u along x and v along y), the GPS subscript represents drifting velocity components obtained from the time derivative of the GPS location measurements, and the Sig subscript represents velocity components from the Signature. Fig. 9 shows vertical profiles of along-channel velocity v averaged along one selected drift (middle) for both flood and ebb tide and the corresponding standard deviation. Only half of the drift was considered for the ebb drift, due to a change in bathymetry about $y = 135$ m (see Fig. 11). The profiles illustrate the spatial variations on the along-channel velocity.

The vertical beam of the Signature provides a direct measurement of the vertical velocities trough the water column. Figs. 10 and 11 show profiles of vertical velocities (averaged to 1 s) along three ebb and three flood drift tracks (shown in Fig. 8).

Vertical velocities range between ± 0.5 m s^{-1}. These profiles illustrate the spatial variations of velocity along different trajectories. During flood, regions of strong vertical velocities ($\sim$0.2 m s^{-1}) are observed along the middle drift trajectory (Fig. 10b). Smaller scale variations are observed along the ebb trajectories. No significant increase in vertical velocity variances is observed near the platform nor in the upper portion of the water column (i.e. no turbulent wake features). For this specific data set, vertical velocity variance is higher along ebb trajectories than along flood trajectories, even if flood currents were stronger.

The turbulent kinetic energy (TKE) dissipation rate, ε, is estimated along each drift through the second-order structure function $D_{LL}(z,r)$ [26]. The structure function is defined as :

$$D_{LL}(z,r) = \overline{[u'(z+r) - u'(z)]^2}, \quad (3)$$

where u' corresponds to a demeaned along-beam velocity, z is the along-beam measurement location, and r is the distance between two along-beam velocity

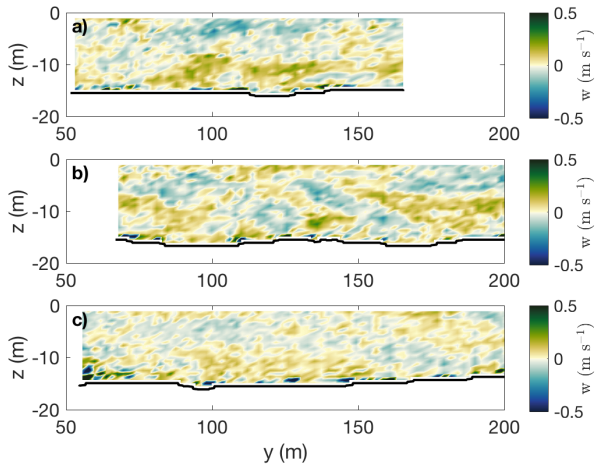

Fig. 10. Vertical and horizontal structure of vertical velocity along three selected drifts during flood tide a) Port, b) Middle, and c) Starboard side of PLAT-I. Black line represents the sea-bottom.

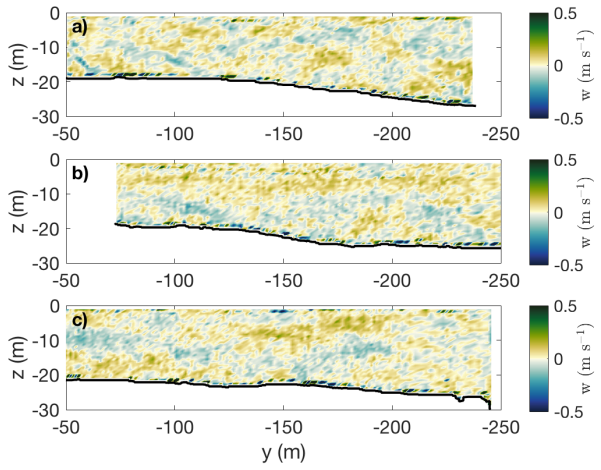

Fig. 11. Vertical and horizontal structure of vertical velocity along three selected drifts during ebb tide a) Port, b) Middle, and c) Starboard side of PLAT-I. Black line represents the sea-bottom.

measurements; the overline denotes a time-average. In the inertial subrange of local isotropic turbulence, the structure function is related to ε by:

$$D_{LL}(z,r) = C_v^2 \varepsilon^{2/3} r^{2/3}, \tag{4}$$

where $C_v^2 = 2.0$ is a constant [27].

The structure function is estimated using 10 s of vertical velocity measurements along the Signature's vertical beam. This window is chosen to minimize the horizontal distance between each velocity profile included in the calculations. Instantaneous measurements are averaged to 1 s to reduce noise. 1 s velocities are demeaned (in time), and velocity differences are calculated at each z for all possible combinations of r, ranging between 1.2 m and 3 m. Velocity differences are then time-averaged over the 10 s. The structure function is linearly fitted to $r^{2/3}$ as:

$$D_{LL}(z,r) = Ar^{2/3} + N, \tag{5}$$

where N is an offset related to the inherent noise of the measurements, and the slope A is used to solve for

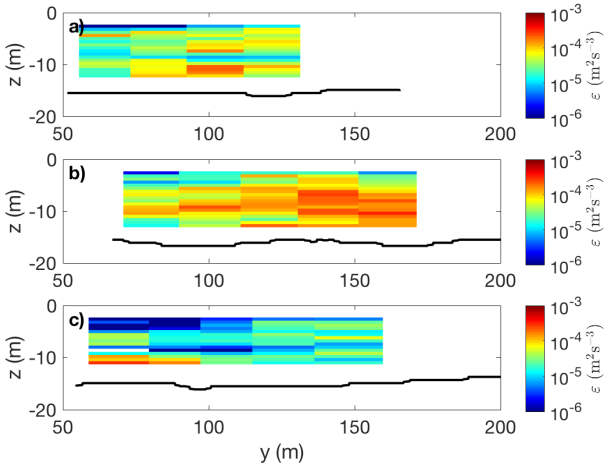

Fig. 12. Vertical and horizontal structure of TKE dissipation rate, ε, along three selected drifts during flood tide a) Port, b) Middle, and c) Starboard side of PLAT-I. Black line represents the sea-bottom.

the dissipation rate as:

$$\varepsilon = \left(\frac{A}{C_v^2}\right)^{3/2} \tag{6}$$

The TKE dissipation rate estimates are presented in Figs. 12 and 13. A large dynamic range is observed in the TKE dissipation rates, illustrating that turbulence varies along each drift track and between them. Although variable, temporal coherence is observed in the TKE dissipation rates along each drift. Observed values are within the range of previous estimates of TKE dissipation rate in Grand Passage using bottom-mounted ADCPs and direct measurements at mid-depth with shear probes [12]. Fig. 14 shows the probability distributions of TKE dissipation rate along the selected transects. The distributions exhibit the log-normal behaviour expected for turbulent flows, and as observed previously in Grand Passage using bottom-mounted ADCP data [28].

The 10 s window used for the TKE dissipation rate calculations is short compared to windows used for turbulence statistics from fixed ADCP measurements in tidal channels [29]. However the observed coherence and log-normal probability distributions indicate the window is sufficient. In the future, the number of profiles used in the TKE dissipation rates estimates will increase by combining data from different drifts at similar locations and tidal stages, following the method presented in [16].

E. Transects

The vessel-mounted RDI Workhorse ADCP provides vertical profiles of horizontal velocity along each transect. Figs. 15 and 16 show vertical profiles of along and across channel velocities respectively. Homogenous velocities are observed along each transect. Along channel velocities are about 2 m s^{-1}. Fig. 17 shows the direction and magnitude of velocity at 6.6 m below the free-surface (approximate hub-depth). Stronger velocities are observed in the downstream transects during ebb, however these were taken an hour earlier than

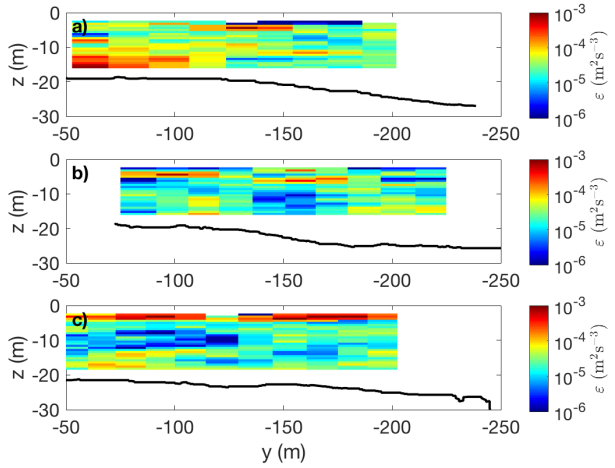

Fig. 13. Vertical and horizontal structure of TKE dissipation rate, ε, along three selected drifts during ebb tide a) Port, b) Middle, and c) Starboard side of PLAT-I. Black line represents the sea-bottom.

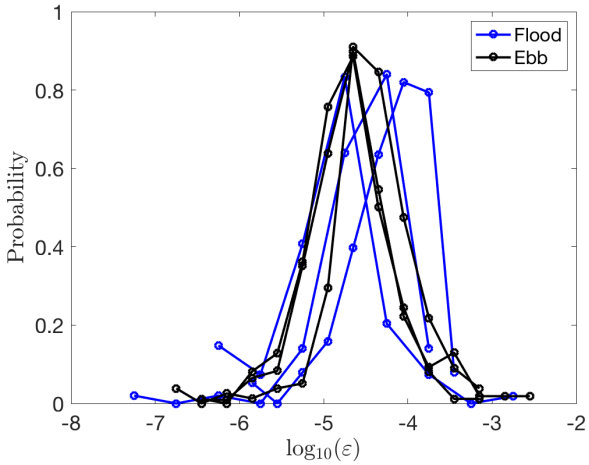

Fig. 14. Probability distribution of $\log_{10}(\varepsilon)$ from selected drifts.

the shown upstream transect, when tides were closer to peak ebb. The velocities are consistent with model predictions shown in Fig. 2. No platform wake features can be observed in these measurements.

IV. Conclusions and Future Work

Spatial mapping of the turbulent flow upstream and downstream PLAT-I tidal energy platform is presented. The methods are proven suitable for capturing both mean flow velocities and resolving turbulence parameters. No significant platform wake signal was observed in the measurements, probably because this is a low blockage situation (turbine blades were not installed), and any effects from the platform structure might be confined to the upper portion of the water column, where velocities are not measured by the down-looking ADCPs, or closer to the platform, where drifter data were contaminated by mooring chain reflection.

Future work will focus on collecting a more extensive data set once the turbine blades are installed and the turbines are operating. All collected data will be organized into a three-dimensional grid and combined to obtain maps of mean-flow velocities and turbulence

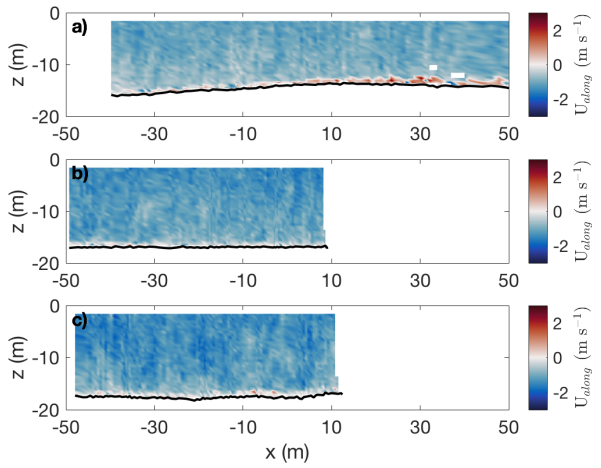

Fig. 15. Vertical and horizontal structure of along-channel velocity at three selected transects during ebb tide: a) upstream ($y \sim 100$ m), b) downstream (D1, $y \sim -40$ m), and c) downstream (D2, $y \sim -70$ m).

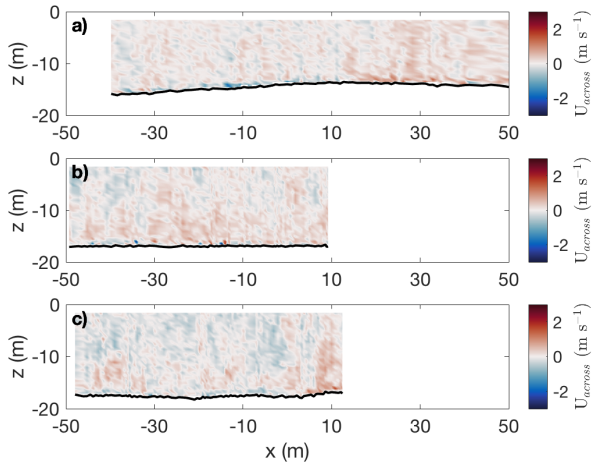

Fig. 16. Vertical and horizontal structure of across-channel velocity at three selected transects during ebb tide: a) upstream ($y \sim 100$ m), b) downstream (D1, $y \sim -40$ m), and c) downstream (D2, $y \sim -70$ m).

parameters for different tidal stages, following the method from [16]. In addition, the data sets will be complemented with concurrent measurements from a bottom-mounted ADCP and a vertical microstructure profiler.

The results from the trial reported here will provide a basis for comparing pre- and post-installation conditions. The combined data set will be used to characterize the structure and extent of the PLAT-I 's wake and to evaluate it's impacts on ambient turbulence levels and flow speeds in Grand Passage.

Acknowledgement

Funding for this investigation has been provided by the Offshore Energy Research Association (OERA) and Canada Foundation for Innovation (CFI). The authors thank the support and collaboration of Sustainable Marine Energy and Black Rock Tidal Power.

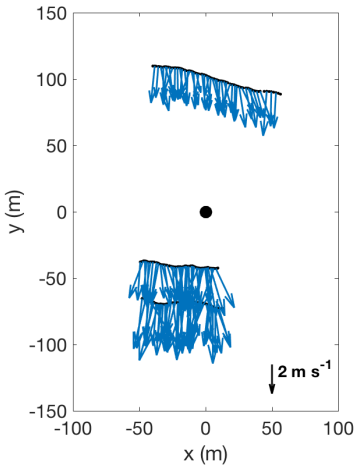

Fig. 17. Velocity direction at selected transects 6.6 m below the free-surface (approximate hub-depth).

REFERENCES

[1] T. Blackmore, L. Myers, and A. Bahaj, "Effects of turbulence on tidal turbines: Implications to performance, blade loads, and condition monitoring," *International Journal of Marine Energy*, vol. 14, pp. 1–26, 2016.

[2] L. Chamorro, C. Hill, S. Morton, C. Ellis, R. Arndt, and F. Sotiropoulos, "On the interaction between a turbulent open channel flow and an axial-flow turbine," *Journal of Fluid Mechanics*, vol. 716, pp. 658–670, 2013.

[3] C. Hill, M. Musa, L. Chamorro, C. Ellis, and M. Guala, "Local scour around a model hydrokinetic turbine in an erodible channel," *Journal of Hydraulic Engineering*, vol. 140, no. 8, p. 04014037, 2014.

[4] R. Cavagnaro, "Impact of turbulence on the control of a hydrokinetic turbine," in *International Conference on Ocean Energy, Halifax, Canada*, 2014.

[5] G. Cada, J. Ahlgrimm, M. Bahleda, T. Bigford, S. Stavrakas, D. Hall, R. Moursund, and M. Sale, "Potential impacts of hydrokinetic and wave energy conversion technologies on aquatic environments," *Fisheries*, vol. 32, no. 4, pp. 174–181, 2007.

[6] G. Boehlert and A. Gill, "Environmental and ecological effects of ocean renewable energy development: a current synthesis," *Oceanography*, vol. 23, no. 2, pp. 68–81, 2010.

[7] M. De Dominicis, R. O. Murray, and J. Wolf, "Multi-scale ocean response to a large tidal stream turbine array," *Renewable Energy*, vol. 114, pp. 1160–1179, 2017.

[8] A. J. G. Brown, S. P. Neill, and M. J. Lewis, "Tidal energy extraction in three-dimensional ocean models," *Renewable Energy*, vol. 114, pp. 244–257, 2017.

[9] Y. Lu and R. Lueck, "Using a broadband ADCP in a tidal channel. Part II: Turbulence," *Journal of Atmospheric and Oceanic Technology*, vol. 16, no. 11, pp. 1568–1579, 1999.

[10] M. Stacey, S. Monismith, and J. Burau, "Measurements of Reynolds stress profiles in unstratified tidal flow," *Journal of Geophysical Research*, vol. 104, pp. 10 935–10 949, 1999.

[11] P. J. Wiles, T. P. Rippeth, J. H. Simpson, and P. J. Hendricks, "A novel technique for measuring the rate of turbulent dissipation in the marine environment," *Geophysical Research Letters*, vol. 33, no. 21, 2006.

[12] J. M. McMillan, A. E. Hay, R. G. Lueck, and F. Wolk, "Rates of dissipation of turbulent kinetic energy in a high Reynolds number tidal channel," *Journal of Atmospheric and Oceanic Technology*, vol. 33, no. 4, pp. 817–837, 2016.

[13] M. Guerra and J. Thomson, "Turbulence measurements from 5-beam acoustic Doppler current profilers," *Journal of Atmospheric and Oceanic Technology*, 2017.

[14] J. Thomson, "Wave breaking dissipation observed with SWIFT drifters," *Journal of Atmospheric and Oceanic Technology*, vol. 29, no. 12, pp. 1866–1882, 2012.

[15] S. F. Zippel, J. Thomson, and G. Farquharson, "Turbulence from breaking surface waves at a river mouth," *Journal of Physical Oceanography*, vol. 48, no. 2, pp. 435–453, 2018.

[16] M. Guerra and J. Thomson, "Wake measurements from a hydrokinetic river turbine," *Renewable Energy*, vol. 139, pp. 483–495, 2019.

[17] L. Myers and A. Bahaj, "Wake studies of a 1/30th scale horizontal axis marine current turbine," *Ocean Engineering*, vol. 34, no. 5, pp. 758–762, 2007.

[18] S. Kang, X. Yang, and F. Sotiropoulos, "On the onset of wake meandering for an axial flow turbine in a turbulent open channel flow," *Journal of Fluid Mechanics*, vol. 744, pp. 376–403, 2014.

[19] L. Chamorro, D. Troolin, S. Lee, R. Arndt, and F. Sotiropoulos, "Three-dimensional flow visualization in the wake of a miniature axial-flow hydrokinetic turbine," *Experiments in Fluids*, vol. 54, no. 2, pp. 1–12, 2013.

[20] P. Bachant and M. Wosnik, "Characterising the near-wake of a cross-flow turbine," *Journal of Turbulence*, vol. 16, no. 4, pp. 392–410, 2015.

[21] M. Rowell, M. Wosnik, J. Barnes, and J. P. King, "Experimental evaluation of a mixer-ejector marine hydrokinetic turbine at two open-water tidal energy test sites in NH and MA," *Marine Technology Society Journal*, vol. 47, no. 4, 2013.

[22] P. Jeffcoate and N. Cresswell, "Field performance testing of a floating tidal energy platform. Part 2: Load performance," in *Proc. 4th Asian Wave and Tidal Energy Conference*, 2018.

[23] J. McMillan, A. Hay, R. Karsten, G. Trowse, D. Schillinger, and M. O'Flaherty-Sproul, "Comprehensive tidal energy resource assessment in the lower Bay of Fundy, Canada," in *Proc. 10th European Wave and Tidal Energy Conference*, 2013.

[24] M. O'Flaherty-Sproul, "New high and low resolution numerical models of the tidal currents through the Digby Neck passages," Master's thesis, Acadia University, 2012.

[25] R. Starzmann, I. Goebel, and P. Jeffcoate, "Field performance testing of a floating tidal energy platform. Part 1: Power performance," in *Proc. 4th Asian Wave and Tidal Energy Conference*, 2018.

[26] S. B. Pope, *Turbulent Flows*. Cambridge University Press, 2000.

[27] K. Sreenivasan, "On the universality of the Kolmogorov constant," *Physics of Fluids*, vol. 7, no. 11, pp. 2778–2784, 1995.

[28] J. M. McMillan and A. E. Hay, "Spectral and structure function estimates of turbulence dissipation rates in a high-flow tidal channel using broadband ADCPs," *Journal of Atmospheric and Oceanic Technology*, vol. 34, no. 1, pp. 5–20, 2017.

[29] K. McCaffrey, B. Fox-Kemper, P. E. Hamlington, and J. Thomson, "Characterization of turbulence anisotropy, coherence, and intermittency at a prospective tidal energy site: Observational data analysis," *Renewable Energy*, vol. 76, pp. 441–453, 2015.